

A Metric for the Quantification of Memory Effects in Power Amplifiers

João Paulo Martins, Pedro Miguel Cabral, Nuno Borges Carvalho and José Carlos Pedro

Abstract—This paper presents a quantitative metric for memory effects in power amplifiers, (PAs), and applies it to various active device technologies and wireless system contexts. The proposed metric is mathematically founded in the dynamic two-tone distortion response, has a clear physical meaning in the important field of PA linearization and can be easily evaluated from either harmonic balance simulations or measurement data gathered in a microwave laboratory. In addition, a memoryless PA linearizer, optimum for reducing the integrated IMD power in the operation bandwidth for a two-tone excitation is derived, providing a rigorous figure of merit of PA linearizability under static IMD compensation. The application of this figure of merit is then illustrated for three different PA prototypes based on Si LDMOS, InGaP/GaAs HBT and GaN HEMT, designed for 900MHz (GSM), 2.1GHz (WCDMA) and 3.5GHz (WiMax) wireless systems, respectively.

Index Terms— long-term memory, memory effects, nonlinear systems, power amplifiers.

I. INTRODUCTION

MEMORY effects, (MEs), have a strong impact on the wireless communication systems performance, since they increase the error vector magnitude of their modulation schemes. Moreover, they are known to impair most common (memoryless) PA linearization techniques. As a result, they have been receiving a large amount of attention from PA design engineers.

Memory effects can be subdivided into two different types of phenomena according to the time constants involved. Short term MEs address time constants of the order of the carrier period and are caused by both the reactive components of the active device and matching networks at the RF band. Since these time constants are much smaller than the ones involved in the information time scale, their effects can be considered as static and the corresponding PAs memoryless.

In contrast, long term MEs are low frequency phenomena (from dc to a few kHz or MHz) involving time constants that are comparable to the information time scale, thus pressing dynamic effects onto the signal's envelope. They are usually attributed to the active device's dynamic thermal effects (i.e., involving some sort of thermal inertia), the active device's charge carrier traps or to the biasing networks [1,2].

Manuscript received March 30, 2006. This work was partially supported by the EU under the Network of Excellence TARGET contract IS-1-507893-NoE and Project ColteMepai POSC/EEA-ESE/55739/2004. The work of J. P. Martins and P. M. Cabral was supported by the Portuguese Science Foundation, F.C.T. under Ph.D. Grants 22056/2005 and 11323/2002, respectively

J. P. Martins, P. M. Cabral, N. B. Carvalho and J. C. Pedro are with Instituto de Telecomunicações, Universidade de Aveiro, 3810-193 Aveiro, Portugal (e-mail: joaoptm@av.it.pt, pcabral@av.it.pt, nborges@det.ua.pt, jcpedro@ieee.org).

From a behavioral point of view, both MEs show up as hysteresis in the AM/AM and AM/PM plots, or as different two-tone intermodulation responses for varying tone spacing [3].

In practice, these MEs play a key role in the PA linearization field since they decrease the performance of most widely used linearization schemes [1,5]. Considering that traditional PA linearizers are designed as memoryless devices, they are ineffective in the presence of IMD dynamics, having no profitable effect on reducing the PAs' distortion power. This is so important that the microwave PA industry has been asking for some form of ME metric capable of evaluating the PA linearizability.

A first attempt to answer this question was addressed by Ku, McKinley and Kenney in [5,6]. In that work, the authors assumed that the best memoryless linearizer was the one that exactly compensates the measured PA AM/AM-AM/PM characteristics. Then the authors defined a metric for memoryless PA linearization as the normalized ratio between the AM/AM-AM/PM response and the deviations of the actual PA two-tone IMD from this AM/AM-AM/PM baseline. Although useful, this metric has been difficult to apply in the industrial environment due to two main reasons.

First, it was conceived and defined under the development of a PA parallel Wiener behavioral model [6]. This gives the impression that it can only be applied after model extraction. Second, and most important, it relies on the assumption that the best memoryless linearizer is the one obtained from the AM/AM-AM/PM characteristics. Effectively, if we recognize that these characteristics are the extrapolated two-tone IMD when the tone separation tends to zero, and considering that the main source of PA memory effects is the inductive bias circuitry, we immediately conclude that such a linearizer is not the best among all the possible memoryless implementations.

In this paper, an in-depth extension of the concept presented in [7] is given and the best memoryless linearizer, BML, theory, for a two-tone excitation, is revisited. Using the two-tone IMD data obtained after the application of this BML linearizer, a new figure of merit was proposed for quantifying memory effects in PAs, which also provides a measure of the PA maximum memoryless linearizability.

To achieve this goal, the two-tone IMD response is first measured over the operation envelope bandwidth. Then this equivalent frequency-domain nonlinear transfer function is converted into a time-domain impulse response, leading to a physical interpretation of the metric's ability to actually characterize the MEs. Finally, this theory is illustrated through its application to different practical PA prototypes.

The paper will thus be organized as follows. First, the BML theory and the memory figure of merit, (MFOM), definition

are presented and discussed in detail, with its validity addressed by simulation. Then we move to the characterization of an in-house built Si LDMOS PA specially designed to include controllable memory effects via an appropriate modification of its bias networks. Next, two different commercial PAs – a WCDMA [8] InGaP/GaAs HBT PA and a WiMax [9] GaN HEMT PA – are measured and evaluated for their memory effects. Note that these results are not meant for any form of comparison between the different PAs - since they were based on different device technologies and conceived for distinct wireless environments - but rather to show the characterization capability of the proposed MFOM for real commercial PAs. Finally, the paper ends summarizing the key conclusions of the developed work.

II. LONG-TERM MFOM REVISITED

In [7], a new figure of merit concept for the evaluation of PA memory effects was proposed enabling the comparison between the linearizability of different PAs. In order to provide a clearer understanding of this MFOM, we first start with a discussion of the memory effects mechanisms arising in a nonlinear PA.

Fig. 1 shows the PA circuit schematic used to model a generic FET based PA.

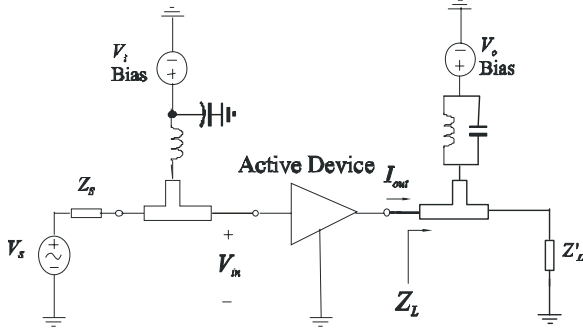


Fig. 1. FET-based PA equivalent circuit diagram used for the theoretical analysis.

Using a Volterra series description, it is possible to relate the intermodulation distortion behaviour with the PA circuit components. Since this type of analysis is well known from previous publications [2,10], only the third-order IMD transfer function, which corresponds to the spectral regrowth at $2\omega_2 - \omega_1$, will be presented:

$$H_3(\omega_2, \omega_2, -\omega_1) = \frac{G_{m3} - 1/3 G_{md} \left[2H_2(\omega_2, -\omega_1)Z_L(\omega_2 - \omega_1) + H_2(\omega_2, \omega_2)Z_L(\omega_2 + \omega_2) \right]}{[1 + G_{ds}Z_L(2\omega_2 - \omega_1)]} \quad (1)$$

where:

$$H_2(\omega_1, \omega_2) = \frac{G_{m2} - 1/2 G_{md} [H_1(\omega_1)Z_L(\omega_1) + H_1(\omega_2)Z_L(\omega_2)]}{[1 + G_{ds}Z_L(\omega_1 + \omega_2)]} \quad (2)$$

$$\text{and } H_1(\omega) = \frac{G_m}{[1 + G_{ds}Z_L(\omega)]} \quad (3)$$

From this simple model, it is easily seen that the output third-order IMD will comprise three different components: one is a direct term arising from G_{m3} that does not depend on $\omega_2 - \omega_1$; a second-order term arising from the $(\omega_1 + \omega_2)$ band, which also does not depend on $\omega_2 - \omega_1$; and finally a term that can be interpreted as an up-conversion of the baseband components back to the fundamental frequencies. This can be represented by the model shown in Fig. 2 [11], where:

$$H_{31}(2\omega_2 - \omega_1) = \frac{G_{m3}}{1 + G_{ds}Z_L(2\omega_2 - \omega_1)} \quad (4)$$

$$H_{22}(\omega_2 + \omega_2) = \frac{-1/3 G_{md} H_2(\omega_2, \omega_2)Z_L(2\omega_2)}{1 + G_{ds}Z_L(2\omega_2 - \omega_1)} \quad (5)$$

and,

$$H_{BB}(\omega_2 - \omega_1) = \frac{-2/3 G_{md} H_2(\omega_2, -\omega_1)Z_L(\omega_2, -\omega_1)}{1 + G_{ds}Z_L(2\omega_2 - \omega_1)} \quad (6)$$

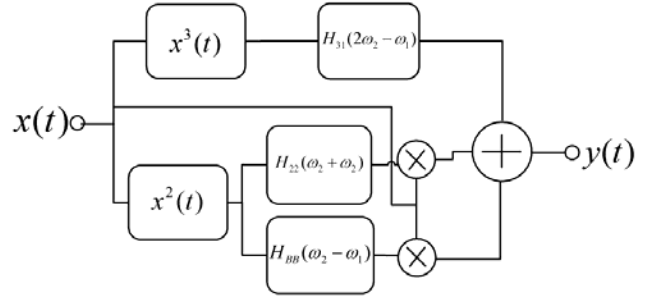


Fig. 2. Model for the PA's long-term memory mechanisms.

Assuming that this PA model is excited by a frequency-domain input signal $x(t) \rightarrow X(\omega)$, the output IMD at $2\omega_2 - \omega_1$ is given by:

$$Y(2\omega_2 - \omega_1) = H_{31}(2\omega_2 - \omega_1)X(\omega_2)X(\omega_2)X(\omega_1)^* + X(\omega_1)^* [H_{22}(2\omega_2)X(\omega_2)X(\omega_2)] + X(\omega_2) [2H_{BB}(\omega_2 - \omega_1)X(\omega_2)X(\omega_1)^*] \quad (7)$$

If we consider $H_{22}(\cdot)$ and $H_{31}(\cdot)$ to be constant with $\Delta\omega = \omega_2 - \omega_1$, then the output IMD variation will only depend on $H_{BB}(\Delta\omega)$, and thus this term will be the exclusive source for the PA long-term memory effects. This assumption is reasonable since, as $\Delta\omega$ varies from DC up to a few MHz, the baseband frequency will vary for some decades, while the second harmonic and the fundamental will only vary a small percentage of the center frequency. This $H_{BB}(\Delta\omega)$ variation

can be attributed to baseband impedance, which occurs, for instance, due to bias networks, thermal effects or trapping. In fact, the most striking factor for the baseband impedance variation is the bias networks, as previously presented in [2].

Important information can be gathered from this model that can be summarized as follows:

- First, if any of the $H_{31}(\cdot)$ or $H_{22}(\cdot)$ terms is significantly larger than the one involving $H_{BB}(\cdot)$, we can be misled by the fact that variation in IMD with $\Delta\omega$ may not be evident, although the PA still presents memory effects that will impair the performance of a memoryless linearizer.
- Second, the IMD asymmetry (different upper and lower IMD components at $2\omega_2 - \omega_1$ and $2\omega_1 - \omega_2$, respectively) only appears when both output impedances at $\omega_2 - \omega_1$ and $\omega_2 + \omega_1$ are complex. In this simple model, this implies that either the in-band direct path or the second harmonic path contributes with a certain amount of imaginary values [2]. This provides a strong insight into these problems, since it states that we can have long-term memory effects even without IMD asymmetry.

One way or the other, the impact of MEs in the PA will limit the use of memoryless linearizers. That is due to the fact that, in a memoryless linearizer, the upper-band IMD is necessarily equal to the lower-band one, and can not track any IMD variation with frequency shown by the PA. In the dynamic IMD case, the upper-band is:

$$Y(2\omega_2 - \omega_1) = K + 2H_{BB}(\omega_2 - \omega_1)X(\omega_2)X(\omega_2)X(\omega_1)^* \quad (8)$$

and the lower-band becomes:

$$Y(2\omega_1 - \omega_2) = K + 2H_{BB}(\omega_2 - \omega_1)^* X(\omega_1)X(\omega_1)X(\omega_2)^* \quad (9)$$

where K is a complex quantity that is constant over the tone spacing.

If we now realize that $X(\omega_1) = X(\omega_2)$, then the difference between the two IMD side-bands come from the addition or subtraction of the imaginary parts of $H_{BB}(\Delta\omega)$ and K , which will imply a different upper and lower IMD value. In order to account for this IMD variation over the operating bandwidth, we should recognize that the term $H_{BB}(\Delta\omega)$ is of foremost importance, since it is the only one that depends on the frequency spacing. Indeed, for capturing those desired MEs, we should neglect the constant part of expression (8) and (9), and retain the only one that changes with the envelope frequency. In expression (7) the constant part corresponds to $H_{31}(\cdot)$ and $H_{22}(\cdot)$, so after the cancellation, only $H_{BB}(\omega_2 - \omega_1)$ will be obtained. This will lead us to the conclusion that although the two-tone IMD must, in general, be modeled through a three-dimensional nonlinear transfer function, it can also be represented via a one-dimensional frequency-domain transfer function of the tone-spacing, $\Omega \equiv \Delta\omega$. In fact, this is the same assumption behind the widely adopted 1st-order

dynamics truncation of the nonlinear integral model [12], or the nonlinear impulse response model [13]. Moreover, it should be said that a swept $\Delta\omega$ two-tone test of a PA around the operating central frequency implicitly assumes this one-dimensional nature. Thus, expression (7) can be viewed as $Y(2\omega_2 - \omega_1) = Y_{IM3}(\Omega) = Y(\omega_2 + \Delta\omega)$, which is the measured (or, possibly, calculated) PA two-tone response used for defining the new ME metric.

The next step consists in defining the best two-tone memoryless linearizer, (BML), of the PA. For that, we assume the general block diagram depicted in Fig. 3, in which the linearizer is used to generate an auxiliary IMD that will compensate the one produced by the stand-alone PA.

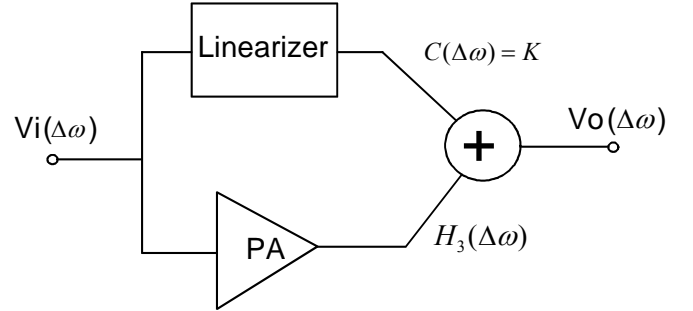


Fig. 3. General PA linearization arrangement.

Note that although Fig. 3 uses a feedforward topology, it can be easily applied to any cascade (pre- or post-distortion) or feedback arrangement, as the output adder does not necessarily stand for any output signal coupler, but for the conceptual addition (in fact, subtraction) of the IMD produced by the PA and its linearizer.

Under this conceptual linearization scheme, we now define the BML for a given PA as the static (or constant with frequency Ω) auxiliary device of Fig. 3 that produces a constant (with tone-spacing) two-tone IMD response, C , that minimizes the distortion power in the considered operation bandwidth, W^l :

$$C : \left[\int_{-W}^{+W} |C - Y_{IM3}(\Omega)|^2 d\Omega \right] \text{ is minimum} \quad (10)$$

From a mathematical viewpoint, this expression states that our memoryless linearizer is a mean-square-error constant estimator, which can thus be determined by:

$$\frac{\partial}{\partial C} \left[\int_{-W}^{+W} |C - Y_{IM3}(\Omega)|^2 d\Omega \right] = 0 \Rightarrow C = \frac{1}{2W} \int_{-W}^{+W} Y_{IM3}(\Omega) d\Omega \quad (11)$$

Therefore, the optimum memoryless linearizer of a certain PA (in a two-tone intermodulation distortion sense) is nothing

¹ Note that, although the following discussion is handled in terms of the actual response, not the transfer function as is more usual, one is easily converted into the other because the response to a unity complex exponential (a unity impulse) is numerically equal to the frequency-domain transfer function (the time-domain impulse response).

more than the system whose constant response is the vectorial mean of the response of that PA to a swept envelope frequency two-tone test, $Y_{IM3}(\Omega)$, within the bandwidth of interest. This constant response can be easily estimated in a microwave laboratory by measuring $Y_{IM3}(\Omega)$ in amplitude and phase over the desired bandwidth.

To get a deeper insight into what such an optimum memoryless linearizer would be, we now turn to the time-domain. For that, we perform the inverse Fourier transform of $Y_{IM3}(\Omega)$ of (11) to obtain:

$$C = \frac{1}{2W} \int_{-W}^{+W} \left[\int_0^{\infty} y_{IM3}(\tau) e^{-j\Omega\tau} d\tau \right] d\Omega = \int_0^{\infty} y_{IM3}(\tau) \text{sinc}(W\tau) d\tau \quad (12)$$

where $\text{sinc}(x) \equiv \sin(x)/x$.

Two limiting situations of the tested $Y_{IM3}(\Omega)$ can be studied. First, we will impose no restriction on the bandwidth, letting $W \rightarrow \infty$. In this case, $\text{sinc}(W\tau)$ becomes a very narrow function (a Dirac delta function) around zero and (12) gives $C = y_{IM3}(0)$. This means that the optimum memoryless linearizer is such that it cancels out the PA instantaneous (or memoryless) IMD, exactly what we were expecting it to do.

Now we consider the opposite situation in which $W \rightarrow 0$. This is the case where C is made equal to $Y_{IM3}(0)$, the AM/AM-AM/PM characteristics. The function $\text{sinc}(W\tau)$ is now a very wide and flat function, and C becomes:

$$C = \int_0^{\infty} y_{IM3}(\tau) d\tau \quad (13)$$

the average of the $y_{IM3}(t)$ impulse response tail.

Thus, the AM/AM-AM/PM linearizer can only be optimum whenever the amplifier is processing a signal whose envelope bandwidth is much smaller than the PA swept tone spacing IMD characteristics, or the temporal IMD dynamics are much slower than the PA memory span.

III. SIMULATED IMPULSE RESPONSE OF THE BML

In order to get a deeper understanding of the BML concept, a harmonic balance simulation was conducted on a simplified PA circuit based on a memoryless transistor model. However, two different bias networks were considered in order to produce different, but controllable memory effects.

A two-tone signal was then used as the input excitation and the output IMD was obtained in magnitude and phase as a function of the input tone separation; see Figs. 4 and 5, respectively.

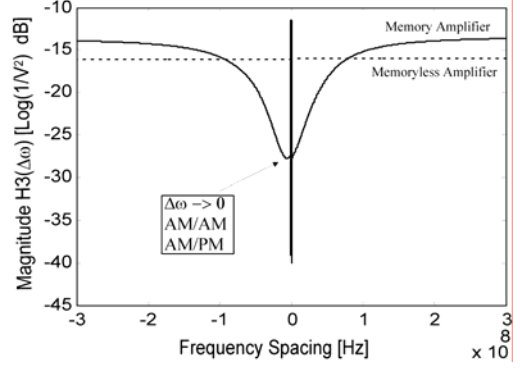


Fig. 4. Simulated IMD magnitude for the memoryless PA and for the PA presenting memory.

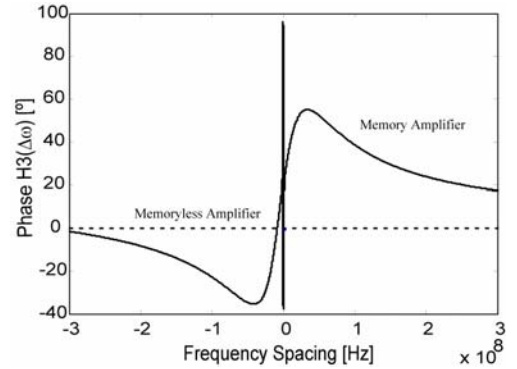


Fig. 5. Simulated IMD phase for the memoryless PA and for the PA presenting memory.

As expected, in the memoryless case, there are no visible changes in both IMD magnitude and phase plots, while in the dynamic case, a large variation with tone spacing is clearly seen. Moreover, the phase shown in Fig. 5 is always zero for the memoryless PA, and something else (not even necessarily anti-symmetrical) when the PA presents memory.

Following the formulation presented in Section II, the BML can be determined from the impulse response's first coefficient, $C = y_{IM3}(0)$, which is equivalent to the average amplitude and phase IMD frequency variation, presented in Figs. 4 and 5, respectively.

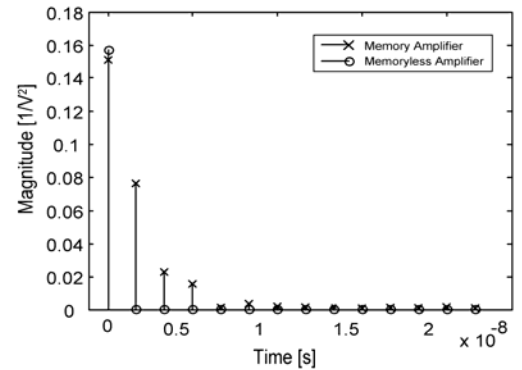


Fig. 6. Impulse response magnitude for the memoryless PA and for the PA presenting memory.

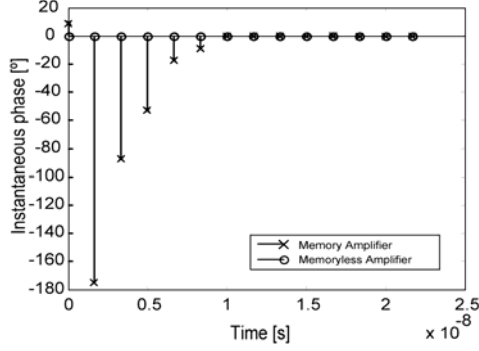


Fig. 7. Impulse response phase for the memoryless PA and for the PA presenting memory.

The impulse response in the memoryless case is a single Dirac delta function at the time origin, see Fig. 6, while in the dynamic case, it expands throughout a certain time span, as expected.

One interesting thing to point out is the complex nature of the obtained impulse response, i.e., that it presents a non-null imaginary part, or a phase that can be something other than zero or 180 degrees, as shown in Fig. 7. Mathematically, this is a consequence of the fact that the frequency response does not present a complex conjugate symmetry with respect to $\Omega = 0$, or that the upper and the lower IMD side-bands are not symmetrical (even symmetry for the amplitude and odd symmetry for the phase). Realizing that $Y_{IM3}(\Omega)$ is the distortion response of the PA to a two-tone, actually a double side-band amplitude modulation with a carrier frequency $\omega_c = (\omega_1 + \omega_2)/2$ and a carrier envelope of frequency $\omega_m = (\omega_1 - \omega_2)/2$ cosine envelope, the amplitude and phase of our impulse response can be interpreted as the evolution in time of the transient response of the AM/AM and AM/PM behavior when the PA is subject to an excitation whose envelope is an ideal impulse. In this sense, it naturally results that the average of the $y_{IM3}(t)$ amplitude is the PA's AM/AM and the non-null average of the $y_{IM3}(t)$ phase is the PA's AM/PM.

Now we compare the performance of our BML with that of the AM/AM-AM/PM static linearizer, respectively obtained from the simulated $Y_{IM3}(\Omega)$ average and the limit of the IMD response when Ω tends to zero, for the dynamic amplifier. Fig. 8 presents the linearizability of the PA presenting memory when both linearizers are used.

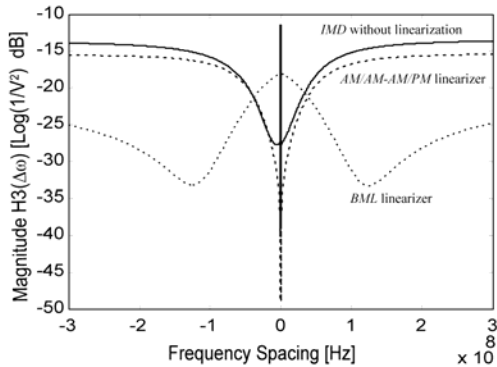


Fig. 8. Linearizability of the PA presenting memory using the AM/AM-AM/PM static linearizer and the now defined BML.

As it can be seen in Fig. 8, the improved quality of the proposed BML approach lies on the better average linearization obtained along the frequency band, when compared with the AM/AM-AM/PM static linearization technique. This directly results from the way the new BML was defined, which is, indeed, optimum for the selected excitation: the standard two-tone stimulus.

IV. MFOM FOR LONG-TERM MEMORY EFFECTS

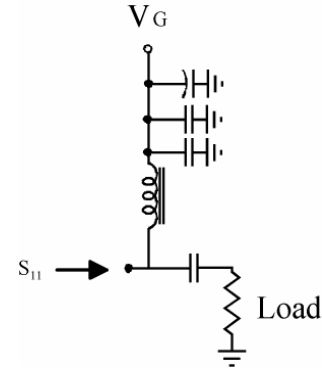
After the explanation of the BML, we are now in a position to define the MFOM of PA linearizability under static conditions [7]. Intuitively, this metric should measure the ratio between the unlinearized IMD integrated power in the desired bandwidth and the total IMD integrated power after memoryless linearization in the same bandwidth²:

$$L_M = \frac{\int_{-W}^{+W} |Y_{IM3}(\Omega)|^2 d\Omega}{\int_{-W}^{+W} |Y_{IM3}(\Omega) - C|^2 d\Omega} \quad (14)$$

Although defined and explained in the frequency domain, such a MFOM can reveal an even more interesting significance when seen in the time domain. For that, we consider again the case where we are interested in the whole PA IMD bandwidth characteristics, i.e., $W \rightarrow \infty$. Since in that case, $C = y_{IM3}(0)$, Parseval's theorem states that our MFOM actually is a metric of the power contained only in the PA dynamic IMD, normalized to the total IMD power. Thus, L_M in (14) is, indeed, a metric of PA long-term memory effects.

V. IN-HOUSE SI-LDMOS PA EVALUATION

In order to validate the proposed theoretical results, a 5W 900MHz Si-LDMOS-based PA for GSM applications [14] was carefully designed using two different bias networks: one memoryless and another one presenting memory in the bandwidth of interest. Fig. 9 presents the generic schematic for both proposed networks.



² The figure of merit definition herein given is the inverse of the one presented in [8], since, this way, it can be more easily interpreted as a metric of the system's linearizability.

Fig. 9. Bias network used in the Si LDMOS-based PA design.

The memoryless bias network was designed to be close to a short circuit in the entire frequency span, while the bias network for dynamic behavior was conceived to present a variable frequency response at baseband. The baseband impedances shown by these two bias networks are depicted in Fig. 10.

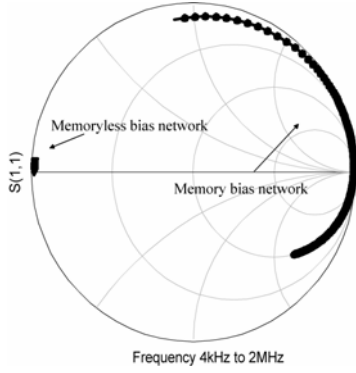


Fig. 10. Measured S_{11} of the bias network.

A two-tone excitation signal was chosen for both the memoryless and the dynamic PA, and the center frequency was set to 900MHz. The tone frequency separation ranged from 4kHz to 2MHz [15]. Figs. 11 and 12 present the measured magnitude and phase values of the one-dimensional 3rd-order transfer function, $H_3(\Delta\omega)$, for both bias network cases.

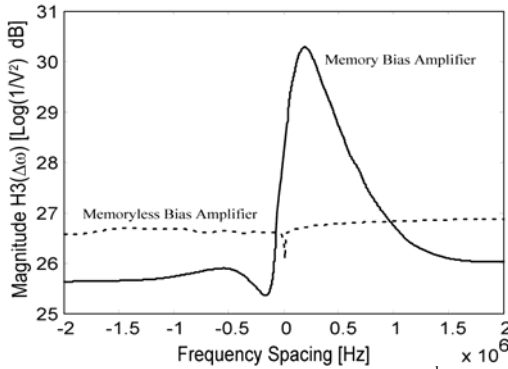


Fig. 11. Measured magnitude values of the 3rd-order transfer function, $H_3(\Delta\omega)$.

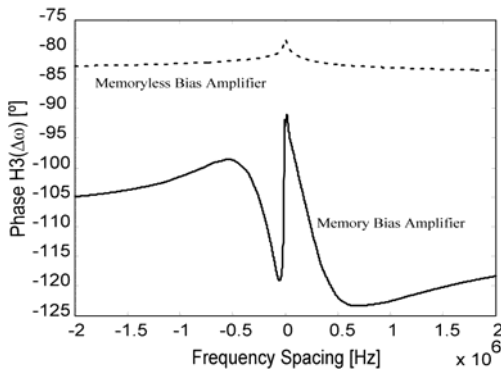


Fig. 12. Measured phase values of the 3rd-order transfer function, $H_3(\Delta\omega)$.

From Figs. 11 and 12, it can be seen that the memoryless PA presents an almost flat magnitude response and a linear phase variation. The corresponding impulse response, obtained from the inverse Fourier transformation of $H_3(\Delta\omega)$, is presented in Figs. 13 and 14, and matches a single Dirac delta defining the BML, as was theoretically predicted.

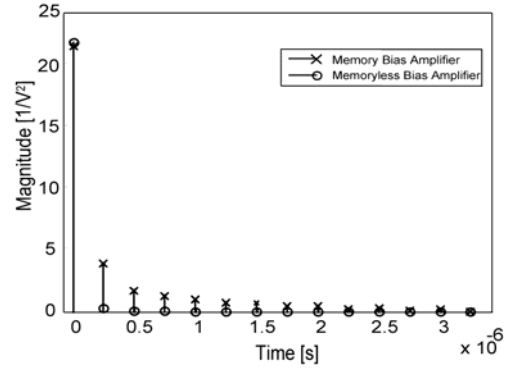


Fig. 13. Measured magnitude values of the 3rd-order transfer function impulse response, $h_3(\tau)$.

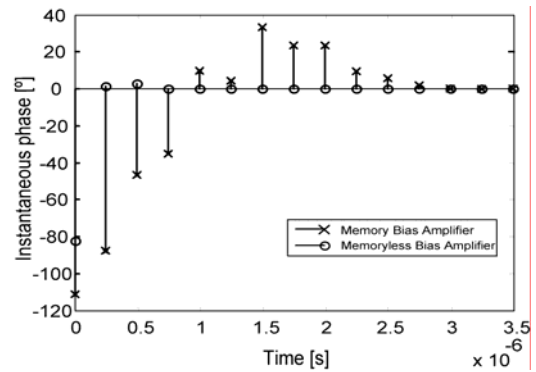


Fig. 14. Measured phase values of the 3rd-order transfer function impulse response, $h_3(\tau)$.

After the linearization procedure using the BML, the intermodulation distortion ratio, IMR, results were compared with the ones obtained before linearization.

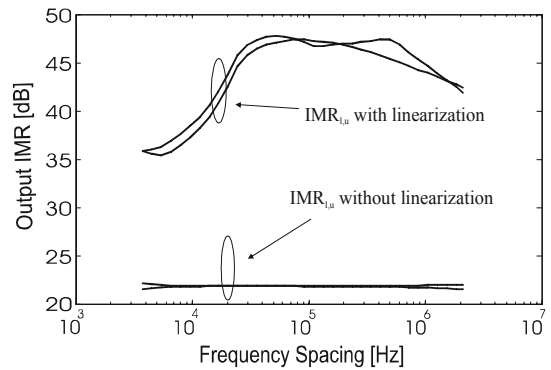


Fig. 15. Measured results of the memoryless Si-LDMOS-based PA, before linearization and after linearization with the BML for both upper and lower sidebands.

Looking at the third order intermodulation ratio, (IMR), linearized response presented in Fig. 15, a residual value of IMR variation can be observed. This could be attributed to dynamic phenomena other than the one determined by the bias networks (e.g., thermal effects). The good performance of the memoryless PA can be seen from the 22.3dB MFOM obtained.

In the dynamic PA case, Figs. 11 and 12, the magnitude and phase of $H_3(\Delta\omega)$ show a variation with frequency spacing that even includes some asymmetry. The impulse response now obtained is no longer a single Dirac delta at $t = 0$, but expands through a certain memory span. But, similarly to what was done before, the BML was still obtained from only the instantaneous value of this response (refer to Figs 13 and 14). After this linearization procedure, the IMR results were once again compared with the ones obtained before linearization, shown in Fig. 16. A visible variation in the IMR response can be noticed both in the linearized and in the non-linearized test.

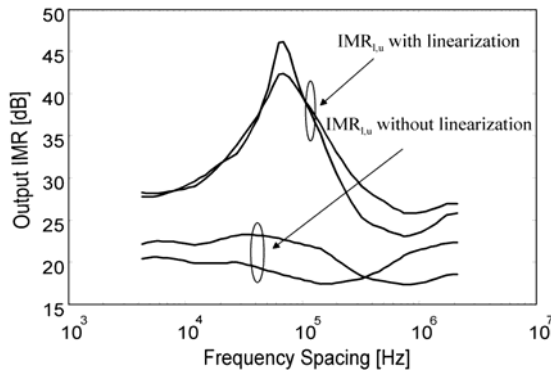


Fig. 16. Measured results of the Si-LDMOS-based PA presenting memory, before linearization and after linearization with the BML for both upper and lower sidebands.

As expected, the memoryless linearizability is now much lower than the one measured for the memoryless PA, as quantified by the obtained MFOM of 7.6dB.

These results show that the memory effects appearing in this PA, due to the bias networks, indeed severely degrade the memoryless linearizability of the proposed design.

VI. MFOM EVALUATION FOR COMMERCIAL PAs

In order to prove the applicability of this new MFOM in real scenarios, the same procedure was followed using two commercial PAs developed for different wireless system applications. The first PA used was a 1.5W, 2.14GHz, InGaP/GaAs HBT-based PA designed for W-CDMA systems [8]. The input excitation used was a two-tone signal with varying tone separation, again from 4kHz to 2MHz. Fig. 17

presents the IMR values obtained before and after the described memoryless linearization procedure³.

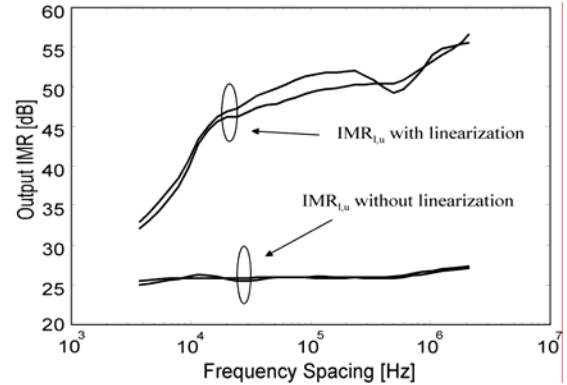


Fig. 17. Measured results of the InGaP/GaAs HBT-based PA, before linearization and after memoryless linearization with the BML for both upper and lower sidebands.

In this case a high value of linearizability could be achieved with this amplifier, expressed by the 24.5dB MFOM obtained.

The second PA used was a 2W, 3.5GHz, GaN HEMT-based PA, intended for WiMax [9], applications. Fig. 18 presents the IMR values obtained before and after the linearization procedure.

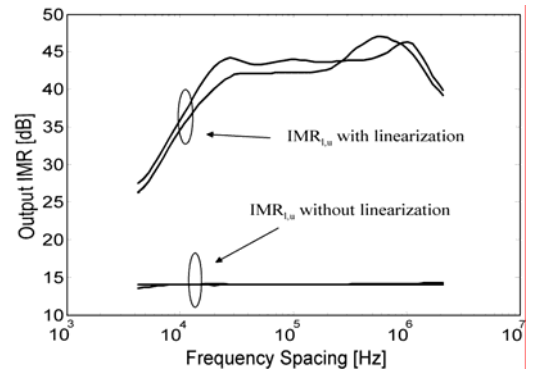


Fig. 18. Measured results of the GaN HEMT based PA, before linearization and after linearization with the BML for both upper and lower sidebands.

In this case, a MFOM of 27 dB was achieved, stating again a high value of memoryless linearizability for this PA.

VII. CONCLUSIONS

This paper presented a metric for the quantification of memory effects in PAs. The proposed metric was given as an intuitive and easily measurable memory figure of merit (MFOM), defined as the unlinearized IMD total power normalized to the IMD power obtained after optimum static linearization. When seen from the time-domain, this MFOM

³ Since the purpose of this experimental section is to demonstrate the ability of the proposed figure of merit to capture the long term memory effects, the amplifiers were operated in a region beyond their rated specifications, in order to show its validity even in limit cases.

can be extremely useful for classify PAs according to their long-term memory effects and memoryless linearizability. In order to obtain this MFOM, a novel two-tone memoryless linearizer norm was also established which proved to be, the best memoryless linearizer under two-tone excitation when compared to other previously proposed alternatives.

Finally, this PA dynamic nonlinearity characterization method was applied to various in-house and commercial PAs, demonstrating its validity.

If a PA is now evaluated using this MFOM, then its linearizability can be easily determined, thus possibly reducing the industry's time to market.

ACKNOWLEDGMENT

The authors wish to acknowledge RFHIC Co., Ltd., WJ Communications, Inc. and Freesacle Semiconductor, Inc. for providing the amplifiers used in this study.

Also, the authors would like to express their gratitude to the reviewers for their comments and suggestions.

REFERENCES

- [1] J. H. K. Vuolevi, T. Rahkonen and J. P. A. Manninen, "Measurement Technique for Characterizing Memory Effects in RF Power Amplifiers," *IEEE Trans. on Microwave Theory and Tech.*, Vol. MTT-49, pp. 1383-1389, 2001.
- [2] N. B. Carvalho and J. C. Pedro, "A Comprehensive Explanation of Distortion Sideband Asymmetries," *IEEE Trans. on Microwave Theory and Tech.*, Vol. MTT-50, pp. 2090 – 2101, Sep. 2002.
- [3] Pedro M. Cabral, Jose C. Pedro and Nuno B. Carvalho, "Dynamic AM-AM and AM-PM Behavior in Microwave PA Circuits", *Asian Pacific Microwave Conference Dig.*, Shanghai, 2005.
- [4] P. B. Kennington, *High-Linearity RF Amplifier Design*, Artech House, Inc. Norwood, MA, 2000.
- [5] A. A. Moulthrop, C. J. Clark, C. P. Silva and M. S. Muha, "A Dynamic AM/AM and AM/PM Measurement Technique," *IEEE MTT-S Intl. Microwave Symposium Dig.*, Vol. 3, pp. 1455–1458, Jun. 1997.
- [6] H. C. Ku, M. D. McKinley and J. S. Kenney, "Quantifying Memory Effects in RF Power Amplifiers," *IEEE Trans. on Microwave Theory and Tech.*, Vol. MTT-50, pp. 2843-2849, Dec. 2002.
- [7] J. P. Martins, N. B. Carvalho and J. C. Pedro, "A Figure of Merit for the Evaluation of Long Term Memory Effects in RF Power Amplifiers," *IEEE MTT-S Intl. Microwave Symposium Dig.*, San Francisco CA, Jun. 2006.
- [8] Universal Mobile Telecommunications System (UMTS), Physical layer, ETSI TS 125 215 V6.4.0.
- [9] IEEE 802.16E-2005 & 802.16/COR1 IEEE Standard for Local and metropolitan area networks.
- [10] J. C. Pedro and N. B. Carvalho, *Intermodulation Distortion in Microwave and Wireless Circuits*, Artech House, Inc., Norwood MA, 2003.
- [11] A. Walker, M. Steer, K. Gard, and K. Gharaibeh, "Multi-Slice Behavioural Model of RF Systems and Devices," *Radio and Wireless Conference Dig.*, pp.71–74, Atlanta, Sep. 2004.
- [12] F. Filicori, G. Vannini and V. Monaco, "A Nonlinear Integral Model of Electron Devices for HB Circuit Analysis,"

IEEE Trans. on Microwave Theory and Tech., Vol. MTT-40, pp.1456-1465, Jul. 1992.

[13] E. Ngoya and A. Soury, "Envelope Domain Methods for Behavioral Modeling", in *Fundamentals of Nonlinear Behavioral Modeling for RF and Microwave Design*, J. Wood and D. Root, Editors, Artech House, Inc., Norwood MA, 2005.

[14] Digital cellular telecommunications system (Phase 2+); Physical layer on the radio path; General description, ETSI TS 100 573 V7.1.0.

[15] J. Martins and N. Carvalho, "Multitone Phase and Amplitude Measurement for Nonlinear Device Characterization", *IEEE Trans. on Microwave Theory and Tech.*, Vol. MTT-53, pp.1982-1989, Jun. 2005.

Copyright 2006 IEEE. Reprinted from IEEE Transactions on Microwave Theory and Techniques

This material is posted here with permission of the IEEE.

Such permission of the IEEE does not in any way imply IEEE endorsement of any of TriQuint Semiconductors' products or services. Internal or personal use of this material is permitted. However, permission to reprint/republish this material for advertising or promotional purposes or for creating new collective works for resale or redistribution must be obtained from the IEEE by writing to pubs-permissions@ieee.org.

By choosing to view this document, you agree to all provisions of the copyright laws protecting it.